GeoAmericas2020
4th PAN AMERICAN CONFERENCE ON GEOSYNTHETICS
26-29 APRIL 2020 • RIO DE JANEIRO • BRAZIL

Effects of Geogrid Aperture Size and Junction Strength on Soil-Aggregate Interface Shear Strength

V.A. Sakleshpur, Lyles School of Civil Engineering, Purdue University, West Lafayette, USA
M.S. Lee, Indiana Department of Transportation, Indianapolis, USA
M. Prezzi, Lyles School of Civil Engineering, Purdue University, West Lafayette, USA
R. Salgado, Lyles School of Civil Engineering, Purdue University, West Lafayette, USA
N.Z. Siddiki, Indiana Department of Transportation, Indianapolis, USA

ABSTRACT
Determination of interface shear strength between soil and geosynthetic reinforcement is critical in the design of many geosynthetic-reinforced soil systems. To study the mechanical interaction between a subgrade soil (glacial till) and an aggregate base (No. 53 aggregate) layer with and without a geogrid at the interface, a series of direct interface shear tests were performed using a large direct shear apparatus. The soil and aggregate layers were prepared at their optimum water contents (16.4% and 8.2% for soil and aggregate, respectively) and compacted in the large direct shear box to relative compaction values of 93–98%. Eight biaxial geogrids with different aperture sizes and junction strengths were used in the direct interface shear tests; each test was performed for three different normal stresses of 50, 100 and 200 kPa. For a given geogrid aperture size, the peak and end-of-test interface shear strength coefficients, defined as the ratio of the shear strength of the soil-aggregate system with a geogrid at the interface to that without a geogrid at the interface corresponding to peak and end-of-test states, respectively, increase with increasing junction strength of the geogrid. Based on the results obtained from this study, the aperture size and normalized aperture size of the geogrid needed to optimize the peak interface shear strength of soil-aggregate-geogrid systems are 28.7 mm and 4.8, respectively, with a minimum junction strength requirement of 11.5 kN/m. These values are restricted to the materials and test conditions used in this study.

1. INTRODUCTION

A stable subgrade foundation is important to ensure a long-lasting pavement structure without excessive deformation and cracking. The lack of strength and stiffness of some foundation soils can present serious problems that can affect the long-term performance of pavements. Weak subgrade soils, such as clay and silt, with high water content can either be completely removed and replaced by properly compacted sandy soils or stabilized chemically by adding a certain percentage by mass of Portland cement, lime, fly ash, slag, or a combination of two or more of these admixtures. However, in urban areas, health concerns due to dust migration may preclude the use of such stabilization methods. Although compaction is usually the least expensive option and is often used to improve subgrade soils, the optimum water content and relative compaction requirements cannot be achieved by compaction methods for clayey and silty soils in areas with high groundwater table. A solution to this problem is to use geogrid reinforcement and replace a portion of the weak subgrade soil with coarse aggregate; this is both a faster and cleaner process than chemical treatment. The geogrid is typically placed at the subgrade-subbase or subgrade-base interface to improve the ability of the weak subgrade to withstand traffic loads without undergoing excessive deformation and to mitigate the development of cracks in the pavement system (Roodi and Zornberg 2012).

Geogrids provide reinforcement by restraining laterally the base or subbase and improve the bearing capacity of the system, thus decreasing the shear stresses on the weak subgrade. The lateral restraint mechanism develops as a result of interface friction and interlocking between the geogrid and the aggregate layer. This interaction between the base aggregate and the geogrid allows the transfer of the shearing load from the base layer to a tensile load in the geogrid. The relatively high tensile stiffness of the geogrid limits the lateral strains in the base layer, and thus produces less vertical deformation of the roadway surface. In addition, the lateral restraint provided by the geogrid increases the mean effective stress of the base course layer leading to an increase in shear strength. Consequently, the ratio of the geogrid aperture size to the aggregate particle size and the confined stiffness of the soil-geosynthetic composite are important parameters that affect the performance of geogrid-reinforced pavement systems (Roodi and Zornberg 2017, Tang et al. 2008, Zornberg et al. 2017). The efficiency of geogrid-reinforced pavement systems is typically evaluated through the interface shear strength coefficient α, which is defined as the ratio of the shear strength $\tau_{reinforced}$ of the subgrade-subbase or subgrade-base system with geogrid reinforcement at the interface to the shear strength $\tau_{unreinforced}$ of the same system but without any geogrid reinforcement, both measured under the same normal stress (Liu et al. 2009, Indraratna et al. 2012, Biabani and Indraratna 2015).

For geomembranes and geotextiles, the interface shear resistance against soil results solely from the frictional resistance mobilized between the reinforcement surface and the soil particles. However, the interaction mechanisms under direct shear mode between soil and geogrids are more complex than those between soil and geosynthetic sheets (Liu et al. 2009). Geogrids are characterized by a combination of longitudinal and transverse ribs. The longitudinal ribs are parallel to the machine direction (roll direction), whereas the transverse ribs are perpendicular to the machine direction. The junctions in a geogrid are the points of intersection of the longitudinal and transverse ribs, as shown in Figure 1. Junction strength is usually defined in terms of the maximum single-junction strength (i.e., the force required to rip the junction apart) and is obtained following the Geosynthetics Research Institute standard GG2 procedure (GRI 1998). It is calculated as

$$T_{j,rib} = \sum_{i=1}^{n} \frac{T_{j,i}}{n} \quad [1]$$

where $T_{j,rib}$ = average single-junction strength (in units of force), $T_{j,i}$ = maximum single-junction strength of each junction (obtained experimentally) and n = number of test specimens. Alternatively, geogrid junction strength is reported in terms of force per unit width of the material, which is the force applied to the junction divided by the nominal aperture opening:

$$T_j = T_{j,rib} N \quad [2]$$

where T_j = geogrid junction strength per unit width (force/unit width) and N = number of junctions per unit width. Regardless of which definition is used, a minimum junction strength is necessary to maintain the integrity of the geogrid during shipment and placement. This is because during pavement construction, the geogrid experiences high levels of localized stresses while the aggregate material is placed, spread and compacted on top of the reinforcement.

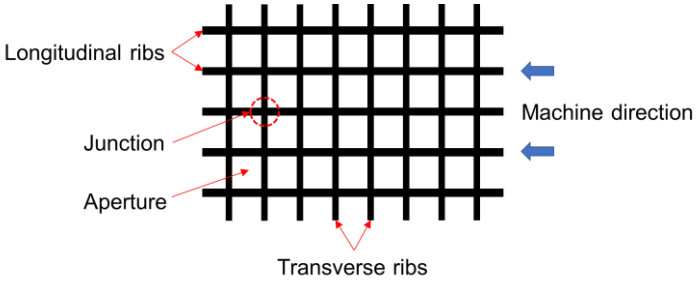

Figure 1. Components of a geogrid.

Although geotextiles and geogrids have been widely used to improve the bearing capacity and reduce excessive vertical deformation and lateral flow of soft subgrade (Perkins and Ismeik 1997, Hufenus et al. 2006), limited studies have examined the influences of geogrid aperture size and junction strength on the behavior of geogrid-reinforced aggregate base-subgrade systems (Sarsby 1985, Tang et al. 2008, Indraratna et al. 2012). Furthermore, no systematic and rigorous studies on the direct interface shear behavior of glacial till-biaxial geogrid-No. 53 aggregate systems have been reported in the literature. Therefore, a series of large-scale direct interface shear tests were performed to investigate the mechanical interaction between subgrade soil (glacial till), biaxial geogrid reinforcement and No. 53 aggregate, and to study the effects of geogrid aperture size and junction strength, among other factors, on the interface shear behavior of this system.

2. MATERIALS

2.1 Subgrade Soil (Glacial Till)

The subgrade soil used in this study is glacial till, which is prevalent in northern and central Indiana, USA. It typically consists of an unsorted, unstratified and heterogeneous mixture of clay-to-boulder sized particles that were deposited by glaciers during the Ice Age. Figure 2 shows the particle size distribution curves for both glacial till (obtained from sieve and hydrometer analyses) and No. 53 aggregate (obtained from sieve analysis), and Table 1 summarizes their properties. Glacial till is classified as CL (sandy lean clay) according to the Unified Soil Classification System (USCS) (ASTM D2487) and as A-4 (moderately plastic silty soil) according to the American Association of State Highway and Transportation Officials (AASHTO M 145). It consists of 32% sand, 48% silt and 20% clay-sized particles by mass with liquid limit of 30.5% and plasticity index of 9.2%. The optimum water content and maximum dry unit weight of glacial till obtained from the results of standard Proctor compaction tests (Method A) (ASTM D698) are 16.4% and 17.5 kN/m^3, respectively. Method A of ASTM D698 consists of compacting the material passing the 4.75 mm sieve in three layers in a 101.6-mm-diameter mold with 25 blows per layer using a 24.5 N rammer dropped from a height of 305 mm. This method was used to compact glacial till because 25% or less by mass of the material was retained on the 4.75 mm sieve (ASTM D698).

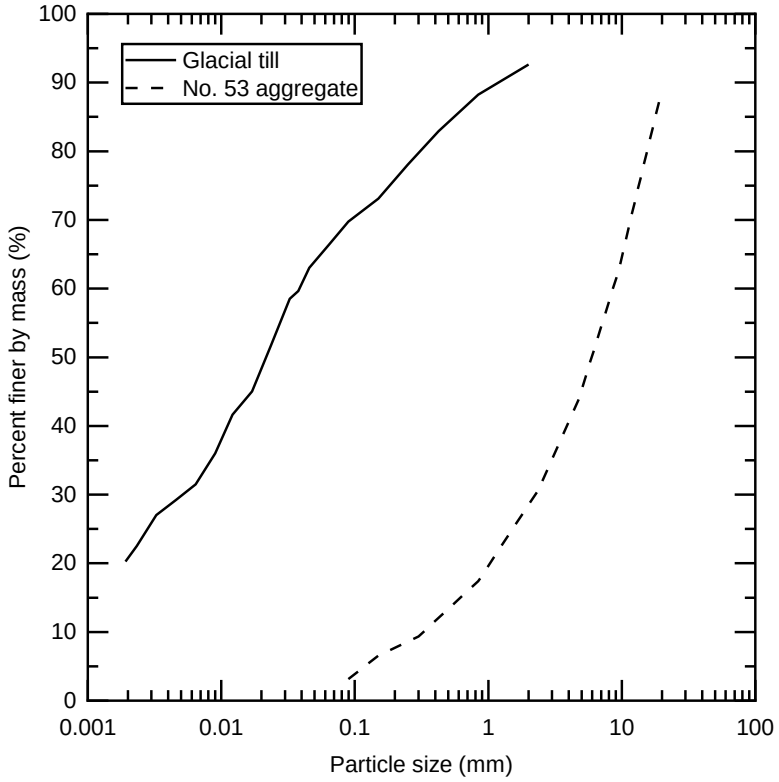

Figure 2. Particle-size distribution curves of glacial till and No. 53 aggregate.

Table 1. Properties of glacial till and No. 53 aggregate.

Property	Glacial till	No. 53 aggregate
Gravel (%)	0	56
Sand (%)	32	42
Fines (%)	68 (48% silt + 20% clay)	2
Mean particle size D_{50} (mm)	0.022	6
Coefficient of uniformity C_U	NA	26.3
Coefficient of curvature C_C	NA	1.75
Liquid limit w_L (%)	30.5	NP
Plastic limit w_p (%)	21.3	NP
Plasticity index I_p (%)	9.2	NP
USCS classification	CL	GW
AASHTO classification	A-4	A-1-a
Optimum water content w_{opt} (%)	16.4	8.2
Maximum dry unit weight $\gamma_{d,max}$ (kN/m^3)	17.5	21.6

Note: NP = non-plastic, and NA = not applicable.

2.2 Base Course Material (No. 53 Aggregate)

No. 53 aggregate (crushed stone) is typically used as the base course material over weak subgrade soils in Indiana, USA. It is classified as GW (well-graded gravel with sand) according to the USCS (ASTM D2487) and as A-1-a (stone fragments or gravel) according to AASHTO M 145. It contains 56% gravel, 42% sand and 2% fines by mass with mean particle size D_{50} of 6 mm. The optimum water content and maximum dry unit weight of No. 53 aggregate obtained from the results of standard Proctor compaction tests (Method C) (ASTM D698) are 8.2% and 21.6 kN/m^3, respectively. Method C of ASTM D698 consists of compacting the material passing the 19 mm sieve in three layers in a 152.4-mm-diameter mold with 56 blows per layer using a 24.5 N rammer dropped from a height of 305 mm. This method was used to compact No. 53 aggregate, as opposed to Method A used for glacial till, because 13% by mass of the material was retained on the 19 mm sieve, which satisfies the gradation criterion for Method C that 30% or less by mass of the material be retained on the 19 mm sieve (ASTM D698).

2.3 Biaxial Geogrid

Eight biaxial geogrids, labelled GGR1 to GGR8, with different aperture sizes and junction strengths were used in this study. Table 2 summarizes the physical and mechanical properties of the geogrids supplied by different manufacturers in the machine direction, which is the direction parallel to the direction of motion of the polymeric material through the processing machine. Geogrids GGR1 to GGR6 were manufactured from polypropylene, whereas geogrids GGR7 and GGR8 were manufactured from polyester. All geogrids had square apertures except for geogrids GGR1 and GGR2 that had rectangular apertures with dimensions of 25 mm and 33 mm in the machine and cross-machine directions, respectively. For geogrids GGR1 and GGR2 with rectangular apertures, the square root of the aperture area was considered as the equivalent aperture size of the geogrid. The aperture size and junction strength of a geogrid affect the frictional resistance mobilized at the soil-aggregate interface because for efficient reinforcement performance, the aggregate particles need to get interlocked within the apertures of the geogrid. Geogrids GGR1, GGR2 and GGR3 have higher junction strengths, whereas geogrids GGR3 and GGR6 have higher aperture sizes than the other geogrids used in this study. Testing of geogrids with different physical and mechanical properties allows one to compare and evaluate experimentally the performance of different geogrid-reinforced soil-aggregate systems.

Table 2. Physical and mechanical properties of the biaxial geogrids in the machine direction.

Property	Geogrid							
	GGR1	GGR2	GGR3	GGR4	GGR5	GGR6	GGR7	GGR8
Aperture area (mm^2)	825	825	1089	225	225	1225	625	625
Aperture size A (mm)	28.7*	28.7*	33.0	15.0	15.0	35.0	25.0	25.0
Tensile strength at 2% strain T_2 (kN/m)[1]	4.1	6.0	4.0	5.0	6.0	15.0	7.7	7.7
Tensile strength at 5% strain T_5 (kN/m)[1]	8.5	11.8	8.0	9.0	12.0	32.0	11.5	15.2
Ultimate tensile strength T_f (kN/m)[1]	12.4	19.2	12.8	13.0	25.0	40.0	34.9	34.9
Junction strength T_j (kN/m)[2]	11.53	17.86	11.90	0.44	0.47	—[3]	0.87	0.87

*Equivalent aperture size (= square root of the aperture area).
[1]Resistance to elongation determined according to ASTM D6637, wherein a geogrid specimen is clamped and subjected to an external tensile force using a constant rate of extension testing machine. The ultimate tensile strength is determined based on the tensile force required to rupture the specimen.
[2]Load transfer capability determined according to GRI-GG2.
[3]Value not reported by the manufacturer.

3. TEST EQUIPMENT AND PROCEDURE

The large direct shear apparatus consists of an upper square box of size 300 mm × 300 mm × 100 mm thick and a lower rectangular box of size 300 mm × 450 mm × 100 mm thick. The plan dimensions of the lower shear box were kept larger than those of the upper shear box in order to maintain a constant shearing area during the tests. The direct interface shear tests were performed according to the following procedure:

(1) The test materials (subgrade soil and base aggregate) were prepared at their optimum water contents. The subgrade soil was compacted in the lower shear box in three layers, as shown in Figure 3(a), to relative compaction (RC) values of 94–98%. The number of blows applied to the first, second and third layers were 280, 330 and 383, respectively, based on the standard Proctor compaction effort.
(2) The geogrid specimen was placed on the compacted subgrade soil and clamped to the lower shear box, as shown in Figure 3(b).
(3) The base aggregate was then compacted in the upper shear box in three layers, as shown in Figure 3(c), to RC values of 93–96%. The number of blows applied to the first, second and third layers were 230, 250 and 370, respectively, based on the standard Proctor compaction effort.
(4) The top cap was placed on the aggregate, as shown in Figure 3(d), and the calibrated load cell and linear variable differential transformer (LVDT) were positioned.
(5) The desired vertical normal stress was applied on the sample and maintained until the vertical displacement had stabilized.
(6) The lower shear box was then displaced horizontally in the machine direction of the geogrid at a constant rate of 1 mm/minute (ASTM D5321) up to a shear displacement of about 83 mm.

Fresh samples of soil and aggregate were compacted for each direct interface shear test. The maximum shear resistance obtained during shearing was recorded as the peak interface shear strength and the shear resistance obtained at the end of the test was recorded as the end-of-test interface shear strength.

(a)

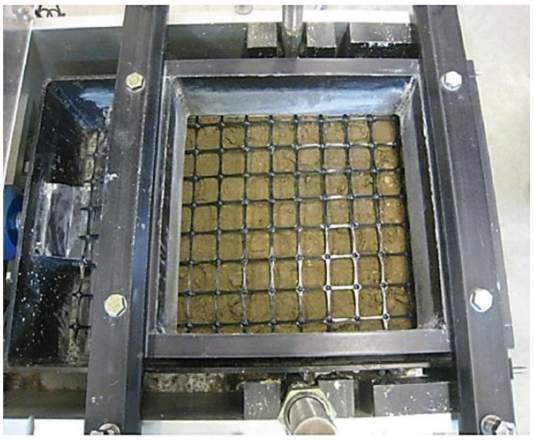

(b)

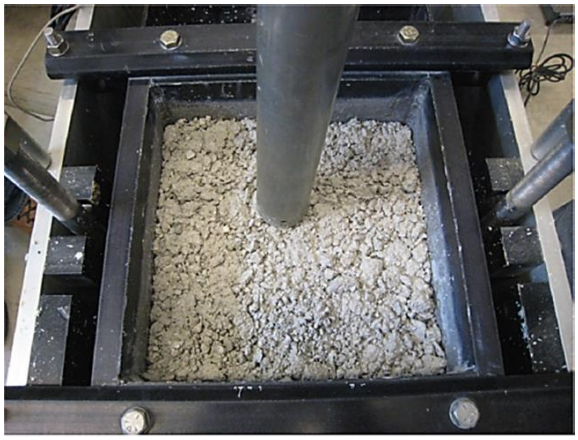

(c)

(d)

Figure 3. Direct shear box setup: (a) subgrade soil placed in lower shear box and compacted in three layers, (b) geogrid placed on compacted subgrade soil and clamped to the lower shear box, (c) aggregate placed in upper shear box and compacted in three layers, and (d) Load cell and LVDT positioned after placement of top cap over aggregate layer.

4. RESULTS AND DISCUSSION

4.1 Test Results

Figures 4(a) and (b) show the shear stress versus shear displacement and vertical displacement versus shear displacement plots, respectively, for the direct interface shear tests performed on both unreinforced and geogrid-reinforced (GGR2, GGR5 and GGR8) soil-aggregate samples subjected to a vertical normal stress of 100 kPa. The GGR2, GGR5 and GGR8 geogrids have different aperture sizes and junction strengths, as shown in Figure 4. The initial stiffness as well as the peak and end-of-test interface shear strengths of the geogrid-reinforced soil-aggregate samples were greater than that of the unreinforced sample. The soil-aggregate sample with geogrid GGR2 placed at the interface exhibited higher peak and end-of-test interface shear strengths than those with geogrids GGR5 and GGR8; the same behavior was also observed when the samples were subjected to 50 kPa and 200 kPa normal stresses. This is attributed to the greater interlocking between the aggregate particles and the apertures of geogrid GGR2 as well as the higher junction strength of GGR2 when compared to geogrids GGR5 and GGR8. The shear displacement required to mobilize the peak interface shear strength is on the order of 30 to 40 mm for the aforesaid geogrid-reinforced samples; however, the unreinforced soil-aggregate sample did not exhibit a distinct peak even up to a shear displacement of 50 mm. Figure 4(b) shows that both the unreinforced and geogrid-reinforced soil-aggregate samples exhibited contractive responses during shearing, and the end-of-test vertical displacements of the geogrid-reinforced soil-aggregate samples were smaller than that of the unreinforced soil-aggregate sample for a vertical normal stress of 100 kPa. Although the direct interface shear tests were performed up to a shear displacement of 83 mm, the test results shown in Figures 4(a) and (b) are limited to a shear displacement of 50 mm because the curves remained quite steady thereafter.

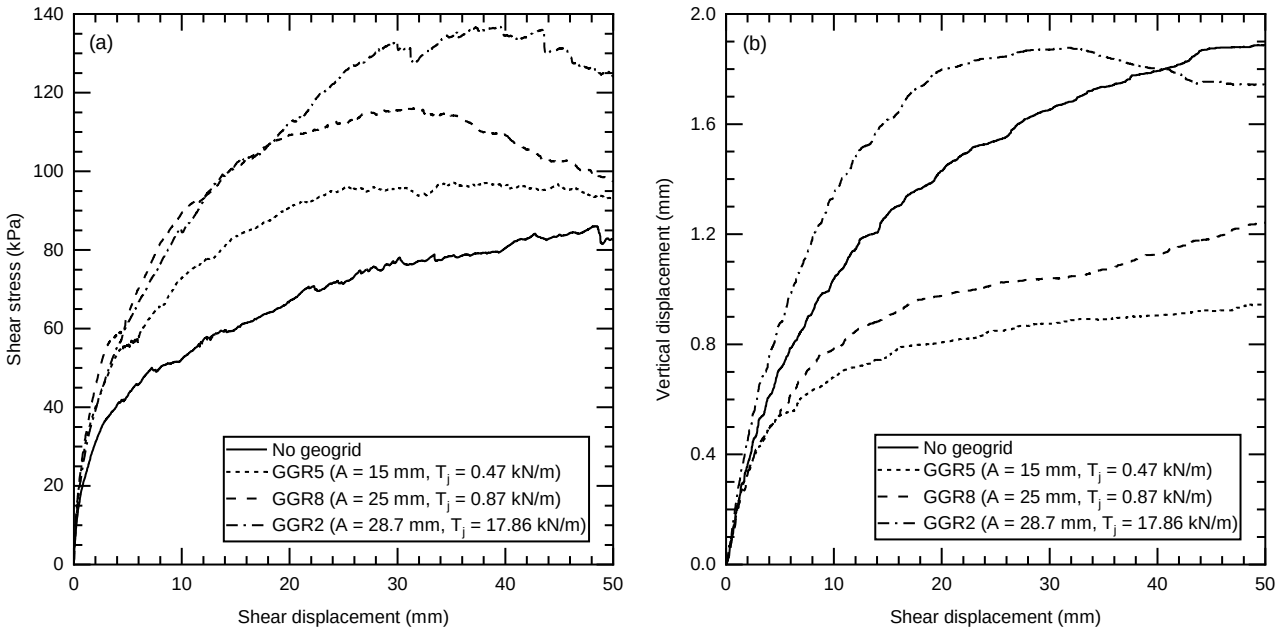

Figure 4. Direct interface shear test results for unreinforced and geogrid-reinforced (GGR2, GGR5 and GGR8) soil-aggregate samples subjected to 100 kPa normal stress: (a) shear stress versus shear displacement curves, and (b) vertical displacement versus shear displacement curves (Note: A = aperture size and T_j = junction strength).

Table 3 summarizes the peak and end-of-test Mohr-Coulomb c-ϕ fitting parameters and the corresponding secant friction angles for a normal effective stress σ'_n of 100 kPa for both unreinforced and geogrid reinforced soil-aggregate samples. The peak c and ϕ values of the unreinforced soil-aggregate sample are 57.0 kPa and 20.1°, respectively, whereas the end-of-test c and ϕ values are 56.1 kPa and 19.2°, respectively. For σ'_n = 100 kPa, the peak and end-of-test secant friction angles of the unreinforced soil-aggregate sample are 40.7° and 40.0°, respectively. The peak and end-of-test secant friction angles were determined by taking the inverse tangent of the ratio of the peak and end-of-test interface shear stresses, respectively, to the corresponding normal effective stress at the soil-aggregate interface. The maximum increase in the peak and end-of-test secant friction angles for the geogrid-reinforced soil-aggregate samples over those of the unreinforced sample are 13.1° for geogrid GGR2 and 8.1° for geogrid GGR6, respectively.

Table 3. Peak and end-of-test c-ϕ fitting parameters and secant friction angles for σ'_n = 100 kPa for soil-aggregate samples tested with and without geogrid reinforcement

Test case	Peak state			End-of-test state		
	Fitting parameters		Secant friction angle for σ'_n = 100 kPa	Fitting parameters		Secant friction angle for σ'_n = 100 kPa
	c (kPa)	ϕ (°)	ϕ_{sec} (°)	c (kPa)	ϕ (°)	ϕ_{sec} (°)
No geogrid	57.0	20.1	40.7	56.1	19.2	40.0
GGR1	111.6	8.8	52.3	78.5	10.0	44.9
GGR2	92.2	24.7	53.8	61.1	26.2	46.2
GGR3	95.0	15.1	48.8	72.0	16.1	46.0
GGR4	57.6	17.7	43.5	46.7	20.7	41.6
GGR5	26.3	35.1	44.2	23.7	34.5	43.6
GGR6	53.4	23.2	48.9	63.0	22.1	48.1
GGR7	89.5	10.5	46.3	73.3	14.0	42.8
GGR8	79.7	15.5	49.2	48.2	21.7	39.5

Tables 4 and 5 summarize the peak and end-of-test interface shear strength coefficients, respectively, for normal effective stresses of 50, 100 and 200 kPa. The average peak and end-of-test interface shear strength coefficients, $\alpha_{p,avg}$ and $\alpha_{eot,avg}$, respectively, calculated for each geogrid as the average of the α_p and α_{eot} values obtained for the three aforesaid normal effective stresses, range from 0.96–1.48 and 0.93–1.21, respectively. The average peak and end-of-test interface shear strength coefficients are lowest for the soil-aggregate-GGR4 interface and highest for the soil-aggregate-GGR2 interface. The average peak and end-of-test interface shear strength coefficients for all the soil-aggregate-geogrid interfaces are greater than unity, except for geogrids GGR4 and GGR8. The main contribution to the shear strength of a soil-aggregate-

geogrid system is particle-grid interlocking, which depends on the size of the geogrid aperture relative to the size of the aggregate particle. If the interface shear strength coefficient is greater than unity, it means that the geogrid is effective in improving the shear strength of the soil-aggregate system due to effective interlocking of the aggregate particles within the geogrid apertures. On the other hand, an interface shear strength coefficient smaller than unity, as obtained for the soil-aggregate-GGR4 and GGR7 interfaces, is attributed to the lack of adequate particle-grid interlocking mainly owing to the inappropriate aperture size of the geogrid relative to the size of the aggregate particles. Tables 4 and 5 also show that the peak and end-of-test interface shear strength coefficients depend on the normal effective stress level at the interface. At lower normal effective stresses, the materials are more dilative, whereas at higher normal effective stresses and larger shear strains, dilation is inhibited. Therefore, depending on the initial sample density, stress state, and degree of interlocking of the aggregate particles within the geogrid apertures, the soil-aggregate-geogrid interaction is expected to be different. The measured interface shear strength coefficients for the soil–aggregate–geogrid samples tested in this study are in good agreement with the range of values reported in the literature: 0.92–1.01 for sand–geogrid interface (Liu et al. 2009), 0.90–1.16 for ballast–geogrid interface (Indraratna et al. 2012), and 1.01–1.29 for subballast (sand + gravel)–geogrid interface (Biabani and Indraratna 2015).

Table 4. Peak interface shear strength coefficients for σ'_n = 50, 100 and 200 kPa.

Geogrid	Aperture size A (mm)	Junction strength T_j (kN/m)	Peak interface shear strength coefficient α_p			$\alpha_{p,avg}$
			σ'_n = 50 kPa	σ'_n = 100 kPa	σ'_n = 200 kPa	
GGR1	28.7	11.53	1.47	1.50	1.07	1.35
GGR2	28.7	17.86	1.45	1.59	1.40	1.48
GGR3	33.0	11.90	1.41	1.33	1.14	1.30
GGR4	15.0	0.44	0.87	1.10	0.90	0.96
GGR5	15.0	0.47	0.76	1.13	1.26	1.05
GGR6	35.0	—	1.05	1.33	1.08	1.16
GGR7	25.0	0.87	1.26	1.22	0.96	1.15
GGR8	25.0	0.87	1.10	1.35	1.00	1.15

Table 5. End-of-test interface shear strength coefficients for σ'_n = 50, 100 and 200 kPa.

Geogrid	Aperture size A (mm)	Junction strength T_j (kN/m)	End-of-test interface shear strength coefficient α_{eot}			$\alpha_{eot,avg}$
			σ'_n = 50 kPa	σ'_n = 100 kPa	σ'_n = 200 kPa	
GGR1	28.7	11.53	1.06	1.18	0.88	1.04
GGR2	28.7	17.86	1.12	1.24	1.26	1.21
GGR3	33.0	11.90	1.06	1.23	1.01	1.10
GGR4	15.0	0.44	0.80	1.06	0.93	0.93
GGR5	15.0	0.47	0.70	1.13	1.25	1.03
GGR6	35.0	—	0.97	1.33	1.10	1.13
GGR7	25.0	0.87	1.11	1.10	0.97	1.06
GGR8	25.0	0.87	0.89	0.98	1.01	0.96

4.2 Effects of Geogrid Aperture Size and Normalized Aperture Size

Figure 5(a) shows the variation of the average peak interface shear strength coefficient $\alpha_{p,avg}$ with the aperture size A of the eight geogrids tested. The average peak interface shear strength coefficient increases with the geogrid aperture size until it attains a maximum value of 1.48 at A = 28.7 mm and then decreases to a value of 1.15 as the value of A approaches 35 mm. A similar trend was reported by Sarsby (1985) for fine sand-geogrid interface and by Indraratna et al. (2012) for ballast-geogrid interface. The $\alpha_{p,avg}$ value is the same for both geogrids GGR7 and GGR8 as they have nearly identical properties. Figure 5(b) shows the variation of $\alpha_{p,avg}$ with the normalized aperture size A/D_{50} of the geogrid; where D_{50} = mean particle size of No. 53 aggregate. Based on the magnitude and trend of $\alpha_{p,avg}$ with A/D_{50}, a zone of effective particle-grid interlock, termed the effective interlock zone (EIZ), is identified between A/D_{50} values of 4.2 and 5.8. In this zone, effective interlocking of relatively larger particles occurs thereby leading to values of $\alpha_{p,avg}$ exceeding unity. The value of $\alpha_{p,avg}$ reaches a maximum of 1.48 at an A/D_{50} ratio of 4.8. For $A/D_{50} < 4.2$, the contribution from the particle-grid interlock is not as significant as that from the interface shear resistance achieved without a geogrid, and thus the values of $\alpha_{p,avg}$ are either less than or close to unity. For $A/D_{50} > 5.8$, the $\alpha_{p,avg}$ values may approach unity, implying that the interface shear behavior may become similar to that of an unreinforced soil-aggregate system, as the geogrid aperture size becomes much greater than the aggregate particle size. Based on these results, it is recommended that the A/D_{50} ratio for glacial till-biaxial geogrid-No. 53 aggregate systems be within the range of 4.2–5.8 with an optimum value of 4.8 in order to maximize the peak interface shear strength. The shear displacement needed to mobilize the interface shear strength associated with $\alpha_{eot,avg}$ may exceed the serviceability requirement of the pavement, and thus more emphasis has been given to $\alpha_{p,avg}$ in the results rather than $\alpha_{eot,avg}$. Although geogrids GGR1 and GGR2 have the same aperture size (= 28.7 mm), the value of $\alpha_{p,avg}$ is greater for GGR2 due to its higher junction strength, as discussed next.

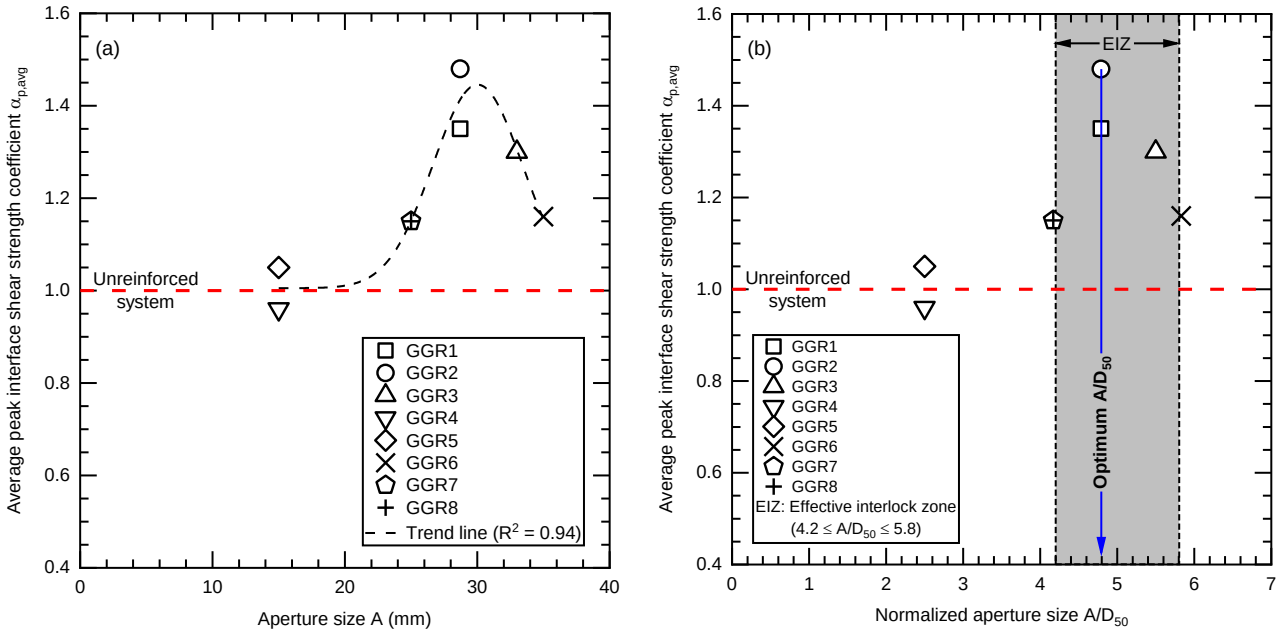

Figure 5. Variation of average peak interface shear strength coefficient with: (a) geogrid aperture size A, and (b) normalized geogrid aperture size A/D_{50}.

4.3 Effects of Geogrid Junction Strength and Tensile Strength at 2% Strain

Figures 6(a) and (b) show the variations of the average peak interface shear strength coefficient $\alpha_{p,avg}$ with the geogrid junction strength T_j and the tensile strength T_2 of the geogrid at 2% strain. The average peak interface shear strength coefficient increases with increasing values of junction strength; the maximum value of $\alpha_{p,avg}$ is 1.48 for geogrid GGR2 with junction strength of about 18 kN/m. On the other hand, there was no clear trend between the tensile strength of the geogrid at 2% strain and the average peak interface shear strength coefficient, as shown in Figure 6(b). This was also the case when the average peak interface shear strength coefficient was plotted against the tensile strength T_5 at 5% strain as well as the ultimate tensile strength T_f of the geogrid.

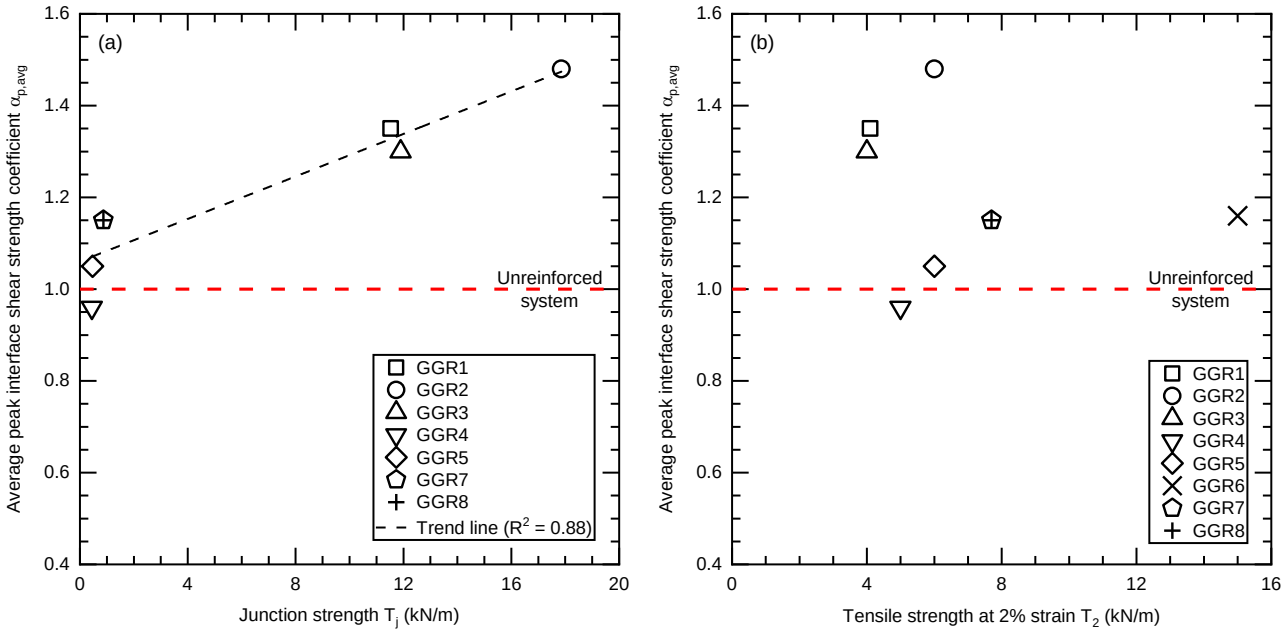

Figure 6. Variation of average peak interface shear strength coefficient with: (a) geogrid junction strength T_j, and (b) tensile strength of geogrid at 2% strain T_2.

4.4 Proposed Equation

Based on the results obtained from the direct interface shear tests performed on the soil-geogrid-aggregate systems considered in this study, it is clear that the average peak interface shear strength coefficient $\alpha_{p,avg}$ depends on the normalized aperture size A/D_{50} and the junction strength T_j of the geogrid. Instead of obtaining an equation between $\alpha_{p,avg}$, A/D_{50} and T_j that does not contain the normal effective stress σ'_n applied to the test samples (which is approximately equal to the vertical effective stress σ'_v acting at the soil-aggregate interface) as a variable, an equation was fitted to the data summarized in Table 4 between parameters α_p, A/D_{50} and T_j for σ'_v = 50, 100 and 200 kPa. The proposed non-dimensional equation for the peak interface shear strength coefficient α_p in terms of A/D_{50} and T_j is

$$\alpha_p = C_1 + C_2\left(\frac{A}{D_{50}}\right) + C_3\left(\frac{T_j}{p_A D_{50}}\right) \quad [3]$$

where p_A = reference stress (= 100 kPa), and C_1, C_2 and C_3 = coefficients that depend on the vertical effective stress σ'_v acting at the soil-aggregate interface. Table 6 summarizes the values of C_1, C_2 and C_3 for σ'_v = 50, 100 and 200 kPa; the corresponding values of the coefficient of determination R^2 and the average relative error between the predicted and measured values of α_p are also included.

Table 6. Values of coefficients C_1, C_2 and C_3 in Eq.3.

Vertical effective stress at soil-aggregate interface σ'_v (kPa)	Coefficient (in Eq.3)			Coefficient of determination R^2	Average relative error (%)
	C_1	C_2	C_3		
50	0.364	0.188	0.006	0.92	5.9
100	0.862	0.099	0.009	0.96	2.4
200	0.937	−0.005	0.013	0.84	5.2

Figure 7 compares the measured values of α_p with those predicted using Eq.3 for σ'_v = 50, 100 and 200 kPa. All the data points lie within ±10% of the measured α_p value except for two outliers (GGR3 at σ'_v = 100 kPa and GGR5 at σ'_v = 200 kPa); these outliers were excluded from the data set that was used to obtain the coefficients in Eq.3. Thus, for A/D_{50} = 2.5–5.8, $T_j/p_A D_{50}$ = 0.7–29.8 and σ'_v = 50, 100 and 200 kPa, Eq.3 can be used to obtain an estimate of the peak interface shear strength coefficient α_p of glacial till-No. 53 aggregate systems reinforced by a biaxial geogrid at the interface. The peak interface shear strength $\tau_{p,reinforced}$ of the glacial till-biaxial geogrid-No. 53 aggregate system can then be obtained by multiplying the value of α_p with the peak interface shear strength $\tau_{p,unreinforced}$ of the same system but without any reinforcement placed at the interface. For intermediate values of σ'_v between 50 and 100 kPa or between 100 and 200 kPa, the values of the coefficients C_1, C_2 and C_3 can be obtained by linear interpolation. An attempt was made to obtain one set of values for the coefficients C_1, C_2 and C_3 applicable for all three vertical effective stresses; however, the resulting value of R^2 was about 0.64 at best, and thus different values of C_1, C_2 and C_3 were proposed for each vertical effective stress in order to obtain a better fit with the measured data.

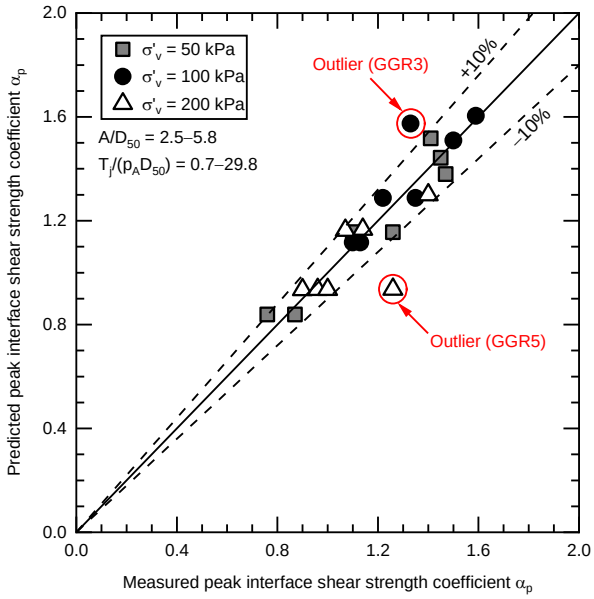

Figure 7. Comparison between predicted and measured values of α_p for σ'_v = 50, 100 and 200 kPa

5. CONCLUSIONS

The responses of various soil-aggregate-geogrid interfaces were investigated through a series of large direct interface shear tests, and interface shear strength coefficients were determined for both peak and end-of-test conditions. The average peak and end-of-test interface shear strength coefficients ranged from 0.96–1.48 and 0.93–1.21, respectively, for the soil (glacial till), aggregate (No. 53 aggregate) and the eight biaxial geogrids considered in this study. The normalized aperture size A/D_{50} and junction strength T_j of the geogrid have a significant influence on the average peak interface shear strength coefficient $\alpha_{p,avg}$. However, no direct correlation was observed between $\alpha_{p,avg}$ and certain geogrid properties, such as the tensile strength at 2% strain, the tensile strength at 5% strain and the ultimate tensile strength. A zone of effective interlocking between the aggregate particles and the geogrid apertures was identified between A/D_{50} values of 4.2 and 5.8, and the optimum geogrid aperture size needed to maximize the peak interface shear strength of glacial till-No. 53 aggregate systems was found to be $4.8D_{50}$. Furthermore, a minimum geogrid junction strength requirement of 11.5 kN/m is recommended based on the results obtained for the eight biaxial geogrids tested. Finally, based on the direct interface shear test results, a non-dimensional equation was developed that can be used to estimate the peak interface shear strength coefficient of geogrid-reinforced glacial till-No. 53 aggregate systems if the geogrid aperture size and junction strength, mean particle size of aggregate, and vertical effective stress acting at the soil-aggregate interface are known. The recommendations and the equation proposed are restricted to the materials and test conditions used in this study.

ACKNOWLEDGEMENTS

This work was supported by the Indiana Department of Transportation through the Joint Transportation Research Program at Purdue University [grant number SPR-3225]. The authors are grateful to the agency for the support. The authors acknowledge the contribution of Yoon Seok Choi for assisting with the laboratory tests. Thanks are also due to Athar Khan for his valuable comments during the course of this study.

REFERENCES

AASHTO M 145. Classification of Soils and Soil-Aggregate Mixtures for Highway Construction Purposes, American Association of State Highway and Transportation Officials, Washington, DC.

ASTM D698. Standard Test Methods for Laboratory Compaction Characteristics of Soil Using Standard Effort (12,400 ft-lbf/ft^3 (600 kN-m/m^3)), American Society for Testing and Materials, West Conshohocken, Pennsylvania, USA.

ASTM D2487. Standard Practice for Classification of Soils for Engineering Purposes (Unified Soil Classification System), American Society for Testing and Materials, West Conshohocken, Pennsylvania, USA.

ASTM D5321. Standard Test Method for Determining the Shear Strength of Soil-Geosynthetic and Geosynthetic-Geosynthetic Interfaces by Direct Shear, American Society for Testing and Materials, West Conshohocken, Pennsylvania, USA.

ASTM D6637. Standard Test Method for Determining Tensile Properties of Geogrids by the Single or Multi-Rib Tensile Method, American Society for Testing and Materials, West Conshohocken, Pennsylvania, USA.

Biabani, M.M. and Indraratna, B. (2015). An evaluation of the interface behavior of rail subballast stabilized with geogrids and geomembranes, Geotextiles and Geomembranes, 43(3): 240-249.

GRI-GG2-87. Geogrid Junction Strength, Geosynthetic Research Institute, Philadelphia, USA.

GRI (1998). GRI Test Methods and Standards, Geosynthetic Research Institute, Drexel University, Philadelphia, USA.

Hufenus, R., Rueegger, R., Banjac, R., Mayor, P., Springman, S.M. and Bronnimann, R. (2006). Full-scale field tests on geosynthetic reinforced unpaved roads on soft subgrade, Geotextiles and Geomembranes, 24(1): 21-37.

Indraratna, B., Hussaini, S.K.K. and Vinod, J.S. (2012). On the shear behavior of ballast-geosynthetic interfaces, Geotechnical Testing Journal, ASTM, 35(2): 305-312.

Liu, C.-N., Zornberg, J.G., Chen, T.-C. and Ho, Y.-H. (2009). Behavior of geogrid-sand interface in direct shear mode, Journal of Geotechnical and Geoenvironmental Engineering, ASCE, 135(12): 1863-1871.

Perkins, S.W. and Ismeik, M. (1997). A synthesis and evaluation of geosynthetic-reinforced base layers in flexible pavements: part I, Geosynthetics International, 4(6): 549-604.

Roodi, G.H. and Zornberg, J.G. (2012). Effect of geosynthetic reinforcements on mitigation of environmentally induced cracks in pavements, 5th European Geosynthetics Congress, Valencia, Spain, 611-616.

Roodi, G.H. and Zornberg, J.G. (2017). Stiffness of soil-geosynthetic composite under small displacements. II: experimental evaluation, Journal of Geotechnical and Geoenvironmental Engineering, ASCE, 143(10), DOI: 10.1061/(ASCE)GT.1943-5606.0001769.

Sarsby, R.W. (1985). The influence of aperture size/particle size on the efficiency of grid reinforcement, 2nd Canadian Symposium on Geotextiles and Geomembranes, Edmonton, Canada, 7-12.

Tang, X., Chehab, G. and Palomino, A.M. (2008). Evaluation of geogrids for stabilising weak pavement subgrade, International Journal of Pavement Engineering, 9(6): 413-429.

Zornberg, J.G., Roodi, G.H. and Gupta, R. (2017). Stiffness of soil-geosynthetic composite under small displacements. I: model development, Journal of Geotechnical and Geoenvironmental Engineering, ASCE, 143(10), DOI: 10.1061/(ASCE)GT.1943-5606.0001768.